Available online at www.sciencedirect.com
ScienceDirect
Journal of Environmental Sciences 2011, 23(7) 1219–1224
JOURNAL OF ENVIRONMENTAL SCIENCES
ISSN 1001-0742
CN 11-2629/X
www.jesc.ac.cn

Preparation of $InYO_3$ catalyst and its application in photodegradation of molasses fermentation wastewater

Zuzeng Qin[1], Yi Liang[1], Zili Liu[1,2,*], Weiqing Jiang[1]

1 School of Chemistry and Chemical Engineering, Guangxi University, Nanning 530004, China. E-mail: qinzuzeng@gxu.edu.cn
2 School of Chemistry and Chemical Engineering, Guangzhou University, Guangzhou 510006, China

Received 08 September 2010; revised 05 December 2010; accepted 09 December 2010

Abstract

An $InYO_3$ photocatalyst was prepared through a precipitation method and used for the degradation of molasses fermentation wastewater. The $InYO_3$ photocatalyst characterized by X-ray diffraction (XRD), UV-Vis diffuse reflectance spectroscopy, surface area and porosimetry. Energy band structures and density of states were achieved using the Cambridge Serial Total Energy package (CASTEP). The results indicated that the photodegradation of molasses fermentation wastewater was significantly enhanced in the presence of $InYO_3$ when compared with $PbWO_4$. The calcination temperature was found to have a significant effect on the photocatalytic activity of $InYO_3$. Specifically, $InYO_3$ calcined at 700°C had a considerably larger surface area and lower reflectance intensity and showed higher photocatalytic activity. The mathematical simulation results indicated that $InYO_3$ is a direct band gap semiconductor, and its conduction band is composed of In 5p and Y 4d orbitals, whereas its valence band is composed of O 2p and In 5s orbitals.

Key words: indium yttrium oxide; molasses fermentation wastewater; photocatalytic degradation

DOI:10.1016/S1001-0742(10)60540-2

Citation: Qin Z Z, Liang Y, Liu Z L, Jiang W Q, 2011. Preparation of $InYO_3$ catalyst and its application in photodegradation of molasses fermentation wastewater. Journal of Environmental Sciences, 23(7) 1219–1224

Introduction

In recent years, there has been an increasing use of ethanol in gasoline. As a result, more ethanol are produced from molasses (a byproduct in the sugar industry and a non-grain material), which generates large volumes of concentrated wastewater that require treatment. This kind of wastewater has bad smell, dark brown color, very high chemical oxygen demand (COD) and high biochemical oxygen demand (BOD_5) (Zeng et al., 2009). This molasses fermentation wastewater contains colored substances, such as melanin derivatives, Maillard pigment, and caramel, as well as large amounts of carbonate and phosphate. Traditional biochemical and physico-chemical treatment methods are inadequate, as these kinds of pigments are heat and light resistant, and they cannot be easily decolorized (Guimarães et al., 1999).

Many techniques have been recently reported for the treatment of this kind of wastewater, such as hydroelectric plasma, TiO_2-catalyzed hydroelectric plasma (Qin et al., 2009c), ozonation and catalyzed ozonation (Coca et al., 2007; Zeng et al., 2009), photocatalytic degradation (Wang et al., 2008; Qin et al., 2009a; Li et al., 2010), wet air oxidation (Arena et al., 2010; Gaálová et al., 2010), and H_2O_2 and H_2O_2/UV processes (Toor and Mohseni, 2007; Kralik et al., 2010). Among these types of methods, advanced oxidative processes will produce hydroxyl radicals (OH·) (Britto and Rangel, 2008; Klavarioti et al., 2009), typically through irradiation of semiconductors with UV light. When the energy of irradiation reaching these semiconductors is sufficient, hydroxyl radicals and super oxide radical ions, which have high activity in the oxidation of organic compounds, are generated.

Yttrium (Y) is a rare earth metal with an outer shell electron distribution of $4d^15s^2$ (i.e., that is, only one d electron exists which can receive pair with other electrons and to form a half-full or full-filled type while maintaining with a stable electron distribution on the yttrium d orbital). In terms of photocatalytic activity, some Y complexes involve complex oxides, such as $TiO_2/YFeO_3$ (Wang et al., 2008), Er^{3+}: $YAlO_3/TiO_2$ (Wang et al., 2010), and $BiYO_3$ (Qin et al., 2009a).

An $InYO_3$ complex oxide was prepared in this study by a precipitation method for photocatalytic degradation of molasses fermentation wastewater. The $InYO_3$ complex oxide was characterized by X-ray diffraction (XRD), UV-Vis diffuse reflectance spectroscopy, surface area and porosimetr, and the effects of calcination temperature on its crystal structure and the photocatalytic activity were

* Corresponding author. E-mail: gzdxlzl@gmail.com

determined.

1 Experiment

1.1 Catalyst preparation and characterization

$In(NO_3)_3$ and $Y(NO_3)_3$ were prepared as 0.1 mol/L aqueous solutions. The $In(NO_3)_3$ solution was added drop wise to the $Y(NO_3)_3$ solution with stirring. The resulting solution was stirred for 30 min to ensure thorough mixing and then adjusted to pH 8 using a 0.5 mol/L NH_4OH, yielding a white precipitate. The precipitate was then filtered and dried at 90°C for 10 hr, resulting in $InYO_3$ precursor. Finally, the precursor was ground and calcined at 600, 700, 800, 900, and 950°C for 2 hr in a muffle furnace to obtain desired $InYO_3$ catalyst.

The $InYO_3$ samples were characterized by X-ray diffraction (XD-3, Beijing Purkinje General Instrument Co., Ltd., China). A diffuse reflection spectrum was obtained using a UV-Vis spectrometer (UV-2501 PC, Shimadzu, Japan) and converted from reflection to absorbance by the Kubelka-Munk method. Geometry optimizations, energy band structures and density of states were calculated using the Cambridge Serial Total Energy package (CASTEP).

1.2 Phtocatalytic degradation of molasses fermentation wastewater

The photocatalytic degradation of molasses fermentation wastewater was performed as a probe reaction to characterize the photocatalytic activity of $InYO_3$. The experiment was carried out in a multi-function photochemical reactor equipped with a 300 W mercury lamp. During the experiment, 200 mL of molasses fermentation wastewater (30-fold diluted) (Qin et al., 2009b) and 2.00 g/L of $InYO_3$ powder were introduced into the reactor. The concentration of molasses fermentation wastewater was then determined by monitoring group absorbance using a dual-beam UV-Vis spectrometer (TU-1901, Beijing Purkinje General Instrument Co., Ltd., China), which was set at an absorption maximum of 475 nm (Coca et al., 2007; Zeng et al., 2009). The concentration of the molasses fermentation wastewater after photocatalytic degradation was calculated by the linear relation between concentration and absorbance.

2 Results and discussion

2.1 Photocatalyst characterization

The XRD patterns of $InYO_3$ prepared by precipitation method from $In(NO_3)_3$ and $Y(NO_3)_3$ and calcined at different temperatures are shown in Fig. 1. Interestingly, the five patterns were basically the same, and the XRD peaks of these five samples could be indexed to bismuth yttrium oxide ($InYO_3$, JCPDS 25-1172), indicating that $InYO_3$ could be prepared by precipitation from $Y(NO_3)_3$ and $In(NO_3)_3$. Subsequent to calcination at 600°C, the crystallization of $InYO_3$ was incomplete, and only some dispersive diffraction peaks were found on the XRD pattern. With the increase in calcination temperature, the

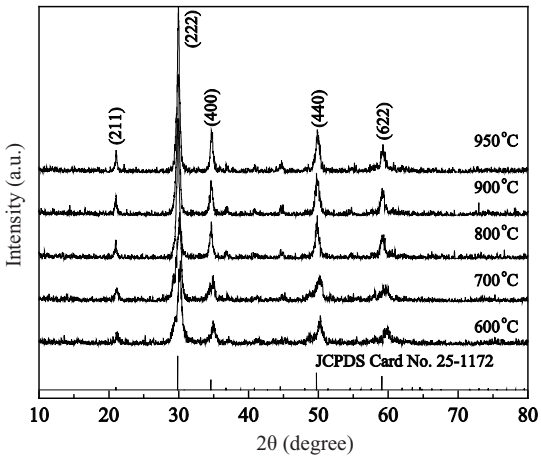

Fig. 1 XRD patterns of $InYO_3$ calcined at different temperatures.

characteristic diffraction peaks of $InYO_3$ were found to become narrower. The diffraction peaks of $InYO_3$ were found to be the narrowest and the highest after calcined at 950°C . As estimated from the full width at half maximum (FWHM) of the $InYO_3$ (222) peak using the Sherrer formula, the particle size of $InYO_3$, which was calcined at 600, 700, 800, 900, and 950°C was found to be 12.4, 14.9, 23.5, 24.8, and 26.8 nm, respectively. Furthermore, the particle size of $InYO_3$ (222-lattice plane) calcined at 600 and 700°C were found to be significantly smaller than those calcined at the other three temperatures. Therefore, higher calcination temperatures were advantageous to crystal growth.

The N_2 adsorption-desorption isotherm and the pore size distribution curve of $InYO_3$ are depicted in Fig. 2a. As can be seen, the N_2 adsorption isotherms of $InYO_3$ calcined at different temperatures belonged to the III-type isotherm with a hysteresis loop. At a relative low pressure ($P/P_0 < 0.8$), there was a gradual increase in the N_2 adsorption process, which indicated transfer from the monolayer adsorption to multilayer N_2 adsorption on the $InYO_3$ catalyst surface (Rouquerol et al., 1999). Regarding desorption, the $InYO_3$ prepared at different temperatures had H3-type hysteresis loops, and the relative pressure of the desorption branches was $0.80 < P/P_0 < 1.0$. This value indicated that the $InYO_3$ prepared at the studied temperatures was sheet material with oblique slit-like holes. It can be seen in Fig. 2 that the start and end of the hysteresis loops of $InYO_3$ calcined at 600°C were the widest, which indicated that the amount of adsorption and desorption was the largest. Therefore, the pore size distribution was most narrow for the catalyst calcined at 600°C.

From the pore size distribution data of $InYO_3$ calcined at different temperatures (Fig. 2b), a limited amount of micropores existed in the $InYO_3$ calcined at 600 and 700°C; however, the amount of this kind of pore is very little. The major pores in these two samples were found to be mesopores with pore size distributions of around 29 and 43 nm, respectively. Most of the pores in $InYO_3$ calcined at 800, 900, and 950°C were found to be mesopores as well, and the pore sizes of these samples were distributed between 10 and 160 nm. In accordance with the N_2 adsorption isotherm-desorption data, the surface area,

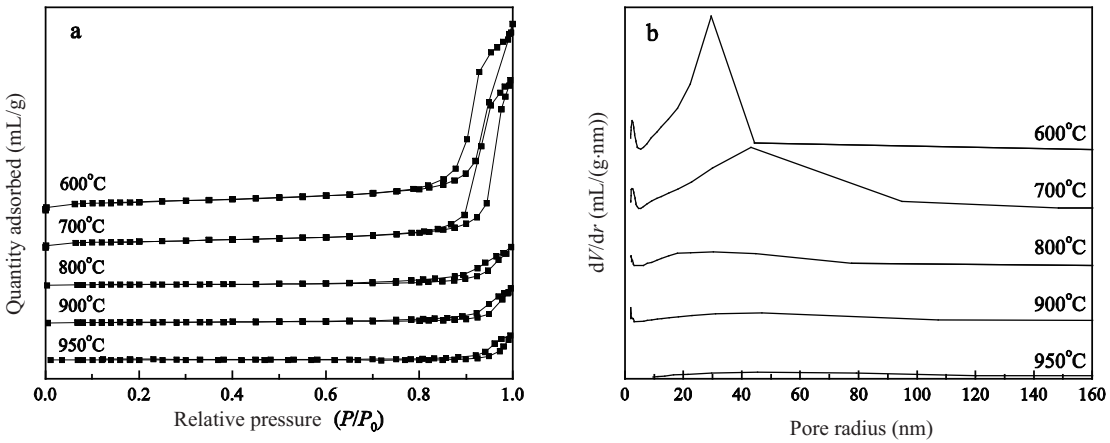

Fig. 2 Effects of calcination temperature on N_2 adsorption-desorption isotherm (a), and the pore size distribution curve of $InYO_3$ (b).

pore volume, and average pore radius from the Brunauer-Emmett-Teller (BET) and Barrett-Joyner-Halenda (BJH) methods are shown in Table 1. From these data, it can be revealed that, with increasing calcination temperature, the surface area of the $InYO_3$ was decreased sharply. Additionally, the surface area and the total pore volume of $InYO_3$ calcined at 600 and 700°C were found to be larger than that calcined at 800 and 900°C. This observation indicated that $InYO_3$ was sintered and the pore structure was destroyed after high temperature calcination.

It can be seen from Fig. 3 that the reflectance spectra of $InYO_3$ calcined at different temperatures were quite similar but that the reflected intensities were different. The light reflectivity of the catalyst calcined at 800°C was found to be the strongest, especially in the visible light range, while that of the catalyst calcined at 700°C was found to be the weakest (i.e., the $InYO_3$ sample calcined at 700°C could absorbe more light in this range).

Table 1 Area-volume summary of $InYO_3$

Calcination temperature (°C)	BET surface area (m^2/g)	Total pore volume (mL/g)	Average pore radius (nm)
600	52.9	0.391	30
700	40.0	0.357	36
800	11.0	0.074	27
900	7.99	0.067	34
950	4.76	0.047	39

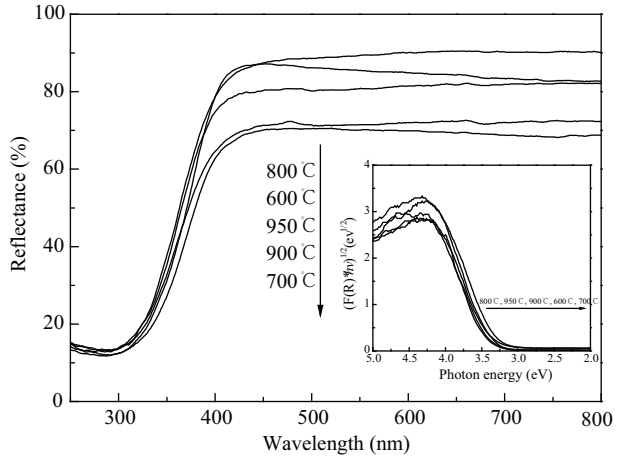

Fig. 3 UV-Visible diffuse reflectance spectra of $InYO_3$, and the absorbance of samples from reflectance by Kubelka-Munkmethod (the inset).

For a semiconductor sample, it is possible to determine the optical absorption near the band edge using the following Eq. (1).

$$ahv = A(hv - E_g)^{n/2} \quad (1)$$

where α, h, v, E_g, and A represent the absorption coefficient, Planck constant, radiation frequency, band gap, and a constant, respectively (Butler, 1977). It can be seen from the inset in Fig. 3 that the absorption edges of the $InYO_3$ calcined at 600, 700, 800, 900, and 950°C were 365, 376, 363, 364, and 363 nm, respectively, and thus the calculated corresponding band gaps were 3.40, 3.30, 3.42, 3.41, and 3.42 eV, respectively.

2.2 Photocatalytic degradation of molasses fermentation wastewater

The time course of photocatalytic degradation for molasses fermentation wastewater in the presence of $InYO_3$ calcined at different temperatures is shown in Fig. 4. After 150 min of photocatalytic reaction with $InYO_3$ calcined at 600, 700, 800, 900, and 950°C, the removal of molasses fermentation wastewater was 90.35%, 98.23%, 81.29%, 73.80%, and 52.37%, respectively. For comparison, the removal of molasses fermentation wastewater under the

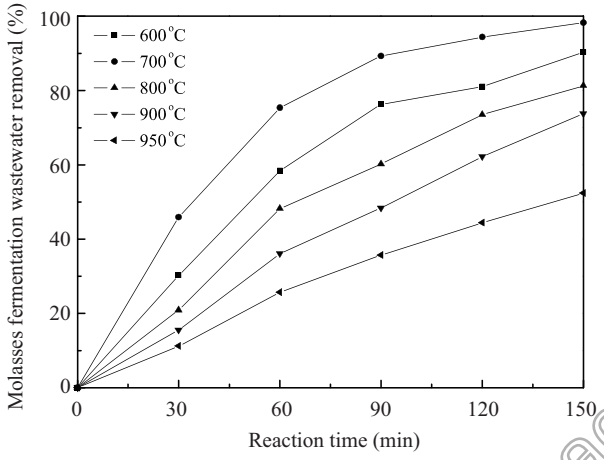

Fig. 4 Molasses fermentation wastewater photocatalytic degradation by $InYO_3$ as catalyst.

same reaction conditions was found to be 90.2% when $PbWO_4$, which prepared by precipitation method, was used as the photocatalyst (Qin et al., 2009b). It can be seen from Fig. 4 that the photocatalytic activity of $InYO_3$ calcined at 700°C was significantly higher than that calcined at 600°C. When combined with the XRD results, it could be concluded that the crystal of $InYO_3$ calcined at 600°C was poor, as some of the crystal phase was not generated, making the photocatalytic activity lower than that catalyst calcined at 700°C. In addition, the photocatalytic activity of $InYO_3$ calcined at 800, 900, and 950°C was also found to be lower than that calcined at 700°C. This phenomenon was explained on the basis that calcination temperatures above 800°C destroyed the pore structure of $InYO_3$ and induced sintering behavior in the crystals, which would cause a decrease in the surface area and pore volume. This decrease of the surface area and pore volume would thus lead to a reduction in the number of crystal defects on the catalyst (Liu et al., 2009), decreasing photocatalytic activity.

It could be observed from the light absorption of $InYO_3$ that the band gap of $InYO_3$ calcined at 700°C was 3.30 eV, which was more narrow than the other four samples. And the absorption edge of $InYO_3$ calcined at 700°C shows a red shift from 363 to 376 nm, indicating that the ability to absorb light of $InYO_3$ calcined at 700°C was the strongest in the five samples. Also, the reflectance of $InYO_3$ calcined at 700°C in the visible light range was found to be lower than the other four samples, indicating that the sample might absorbe more visible light. The increasing ability to absorb light of $InYO_3$ calcined at 700°C improved charge separation and inhibition of charge carrier recombination, which is essential in enhancing the overall quantum efficiency of the photodegradation process and increasing the photocatalytic activity (Carp et al., 2004).

The experimental data in Fig. 4 were fit to a plot of $-\ln(c/c_0)$ versus reaction time (t) to investigate the kinetics of the photocatalytic degradation of molasses fermentation wastewater by $InYO_3$ calcined at different temperatures; The results of the kinetics in Table 2 were found to be consistent with the first-order law equation (Eq. (2)):

$$-\frac{dC}{dt} = k'C \quad (2)$$

where, k' and C represent the reaction rate constant, and the concentration of wastewater, respectively. In addition, the correlation coefficients, R^2, indicated that the data fit reasonably well with this pseudo first-order model. Therefore, it could be concluded that the process of photocatalytic degradation of molasses fermentation wastewater by $InYO_3$ calcined at different temperatures involved pseudo first-order reactions kinetics. The rate constants in Table 2 also indicates the photocatalytic activity of the samples, the rate constant of the photocatalytic degradation of molasses fermentation wastewater with $InYO_3$ calcined at 700°C was 26.47×10^{-3} min^{-1}, which was the highest among the samples.

Since molasses fermentation wastewater has a high chemical oxygen demand (COD), the COD_{Cr} of wastewater was also studied using $InYO_3$ as a photocatalyst (Table 2). The COD_{Cr} of molasses fermentation wastewater in this study was as high as 4.53×10^3 mg/L, even after 30-fold dilution. However, when using $InYO_3$ calcined at 700°C for 2 hr as the photocatalyst, the COD_{Cr} of 30-fold diluted molasses fermentation wastewater after a 150 min photocatalytic reaction was significantly reduced to 0.32×10^3 mg/L (i.e., a reduction of 92.98%). This drop in COD_{Cr} reflected the degradation of complex organic compounds into small molecules, such as CO_2 and H_2O. Thus, the decolorization of the wastewater was accompanied by a significant reduction in COD_{Cr}.

2.3 Mathematical simulation of the band gap

The spectral properties of semiconductor are mainly based on their energy band structure. At present, the valence band structure of simple crystals can be calculated by theoretical simulations. Based on the density functional theory, the valence band structure, conduction band, and density of states of $InYO_3$ can be calculated using the CASTEP module of Material Studio, which based on Density Functional Theory (DFT). The calculated electronic band structure and the partial density of states of $InYO_3$ are plotted in Fig. 5.

In the calculation, the crystal structure of $InYO_3$ was first geometry optimized, and then the energy band structure and density of states (including the total density of states and the partial density of states) were calculated. The calculations indicated that $InYO_3$ is an indirect gap crystal, and that the direct gap at 2.6 eV, which is mainly caused by the 3d states of Y and the 2p of O, was 0.66 eV lower than the indirect gap (2.14 eV).

$InYO_3$ is a direct band gap semiconductor, as its conduction band is mainly composed of In 5p and Y 4d orbital, whereas its valence band is composed of O 2p and In 5s

Table 2 Degradation rate as function of calcinations temperature and pseudo-first order rate constants derived form fitting experimental data to computer model and the photocatalytic degradation activities of $InYO_3$

Calcination temperature (°C)	Rate constant (10^{-3} min^{-1})	R^2	Decolorization of molasses fermentation wastewater (%)	COD_{Cr} ($\times10^3$ mg/L)	COD removal (%)
Before reaction	–	–	0	4.56	0.00
No catalyst	–	–	0.98	4.53	0.66
600	15.40	0.987	90.35	0.94	79.39
700	26.47	0.990	98.23	0.32	92.98
800	11.36	0.994	81.29	2.88	36.84
900	8.88	0.983	73.80	3.24	28.95
950	5.01	0.998	52.37	3.52	22.81

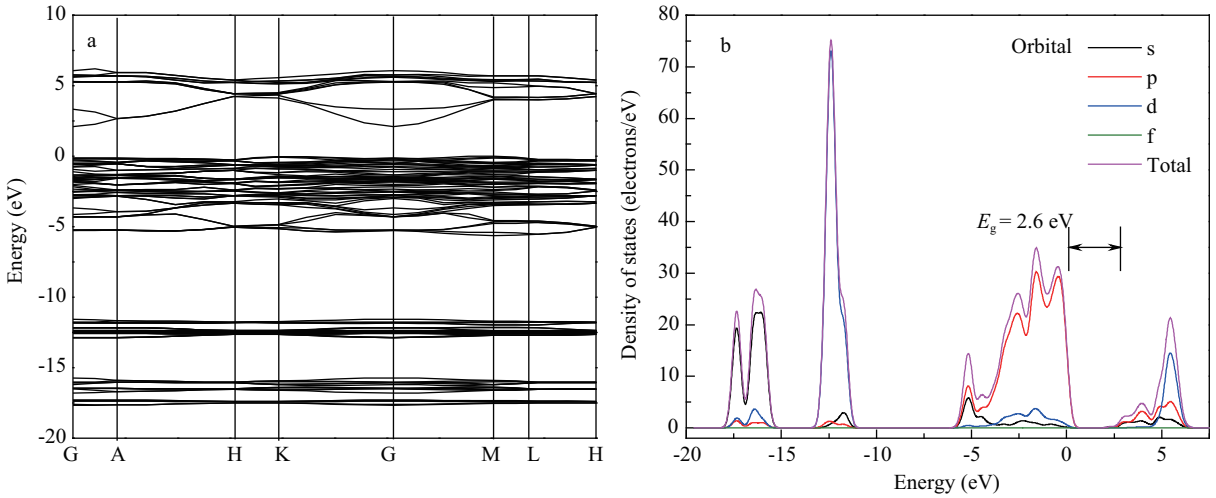

Fig. 5 Electronic band structure (a) and partial density of states (b) of $InYO_3$.

orbital. The band gap between the conduction band and the valence band was found to be about 2.60 eV. This calculated gap (2.60 eV) was a 0.8 eV lower than the measured optical band gap (3.40 eV). This discrepancy could result because of the following reasons (Hohenberg and Kohn, 1964; Zhang et al., 2008; Xie et al., 2002). (1) In the CASTEP method, the "pseudo-potential", which contains several parameters, is used to approximately describe the potential energy field of electrons in the crystal. (2) Systematic errors may result from local density approximation and generalize gradient approximation of the electronic interaction. (3) The result calculated by density functional theory is an approximation result at 0 K, which may lead to differences in the experimental results obtained at atmospheric temperature. (4) The intrinsic value of the K-S equation in the local functional theory does not provide the energy of the system in the excited state, which may result in the theoretical band gap value that is 30%–50% lower than the experimental value. Despite these differences, the theoretical values reported here would be helpful for understanding the absorption properties and the electric excitation and the transfer of $InYO_3$ in the photocatalytic process.

3 Conclusions

The results obtained in the present study indicated that $InYO_3$ synthesized by precipitation methods could serve as promising and efficient photocatalysts for the degradation of organic compounds. With $InYO_3$ calcined at 700°C as the photocatalyst, molasses fermentation wastewater was efficiently degraded. After 150-min photocatalytic reaction, the decolorization and COD removal of molasses fermentation wastewater were 98.23% and 92.98%, respectively.

Acknowledgments

This work was supported by the National Natural Science Foundation of China (No. 21006013) and the Scientific Research Foundation of Guangxi University (No. XBZ090780).

References

Arena F, Italiano C, Raneri A, Saja C, 2010. Mechanistic and kinetic insights into the wet air oxidation of phenol with oxygen (CWAO) by homogeneous and heterogeneous transition-metal catalysts. *Applied Catalysis B: Environmental*, 99(1-2): 321–328.

Britto J M, Rangel M D C, 2008. Advanced oxidation process of phenolic compounds in industrial wasterwater. *Quimica Nova*, 31(1): 114–122.

Butler M A, 1977. Photoelectrolysis and physical properties of the semiconducting electrode WO_3. *Journal of Applied Physics,* 48(5): 1914–1920.

Carp O, Huisman C L, Reller A, 2004. Photoinduced reactivity of titanium dioxide. *Progress in Solid State Chemistry*, 32(1-2): 33–177.

Coca M, Pena M, Gonzalez G, 2007. Kinetic study of ozonation of molasses fermentation wastewater. *Journal of Hazardous Materials,* 149(2): 364–370.

Gaálová J, Barbier Jr J, Rossignol S, 2010. Ruthenium versus platinum on cerium materials in wet air oxidation of acetic acid. *Journal of Hazardous Materials*, 181(1-3): 633–639.

Guimarães C, Bento L S M, Mota M, 1999. Biodegradation of colorants in refinery effluents: potential use of the fungus *Phanerochaete chrysosporium*. *International Sugar Journal*, 101(1205): 246–251.

Hohenberg P, Kohn W, 1964. Inhomogeneous electron gas. *Physical Review*, 136(3B): B864–B871.

Klavarioti M, Mantzavinos D, Kassinos D, 2009. Removal of residual pharmaceuticals from aqueous systems by advanced oxidation processes. *Environment International,* 35(2): 402–417.

Kralik P, Kusic H, Koprivanac N, Loncaric Bozic A, 2010. Degradation of chlorinated hydrocarbons by UV/H_2O_2: The application of experimental design and kinetic modeling approach. *Chemical Engineering Journal*, 158(2): 154–166.

Li Y J, Chen J, Liu J B, Ma M Y, Chen W, Li L Y, 2010. Activated carbon supported TiO_2-photocatalysis doped with Fe ions of continuous treatment of dye wastewater in a dynamic reactor. *Journal of Environmental Sciences*, 22(8): 1290–1296.

Liu Z L, Li H, Qin Z Z, Chen S Z, Ke G, Chen G S et al., 2009. Photocatalytic activity of $BiVO_4$ and its positron annihilation spectrum. *Chemical Industry and Engineering Progress*, 28(5): 904–907.

Qin Z Z, Liu Z L, Liu Y B, Yang K D, 2009a. Synthesis of $BiYO_3$ for degradation of organic compounds under visible light irradiation. *Catalysis Communications*, 10(12): 1604–1608.

Qin Z Z, Liu Z L, Yang K D, Wei J H, 2009b. Degradation of molasses fermentation wastewater by $PbWO_4$ photocatalyst. *Journal of Chemical Engineering of Chinese Universities*, 23(2): 339–344.

Qin Z Z, Liu Z L, Zeng Y F, Sun J H, Yang K D, 2009c. The effects of different methods of catalyst preparation on the hydro-electric plasma TiO_2-catalyzed degradation of 2,4-dinitrophenol. *Environmental Chemistry Letters*, 7(2): 149–153.

Rouquerol F, Rouquerol J, Sing K, 1999. Adsorption by Powders and Porous Solids, Principles, Methodology and Applications. Academic Press, San Diego. 93–114.

Toor R, Mohseni M, 2007. UV-H_2O_2 based AOP and its integration with biological activated carbon treatment for DBP reduction in drinking water. *Chemosphere,* 66(11): 2087–2095.

Wang W C, Li S, Wen Y Y, Gong M C, Zhang L, Yao Y L et al., 2008. Synthesis and characterization of TiO_2/$YFeO_3$ and its photocatalytic oxidation of gaseous benzene. *Acta Physico-Chimica Sinica,* 24(10): 1761–1766.

Wang J, Xie Y, Zhang Z, Li J, Li C, Zhang L et al., 2010. Photocatalytic degradation of organic dyes by Er^{3+}:$YAlO_3$/TiO_2 composite under solar light. *Environmental Chemistry Letters*, 8(1): 87–93.

Xie C K, Xu P S, Xu F Q, Pan H B, 2002. Theoretical calculations on the atomic and electronic structure of beta-SiC(110) surface. *Chinese Science Bulletin*, 47(5): 804–809.

Zeng Y F, Liu Z L, Qin Z Z, 2009. Decolorization of molasses fermentation wastewater by SnO_2-catalyzed ozonation. *Journal of Hazardous Materials*, 162(2-3): 682–687.

Zhang F C, Zhang Z Y, Zhang W H, Yan J F, Yun J N, 2008. The first-principle calculation of electronic structure and optical properties of In_2O_3. *Acta Chimica Sinica*, 66(16): 1863–1868.